J Seismol (2012) 16:733–743
DOI 10.1007/s10950-012-9297-4

ORIGINAL ARTICLE

Comparison of point and array-computed rotations for the TAIGER explosions of 4 March 2008

Lauren M. Kendall · Charles A. Langston · W. H. K. Lee · C. J. Lin · C. C. Liu

Received: 1 August 2011 / Accepted: 9 March 2012 / Published online: 3 April 2012

Abstract Two large explosions were recorded by a dense array of strong-motion accelerometers and rotational seismometers in northeastern Taiwan associated with a Taiwan Integrated Geodynamics Research long-range refraction experiment. The objective of this experiment was to test the response of the experimental eentec rotational seismometers against calculated array rotations. Computed array rotation rates are seen to have little variation across the array, but point rotation rate measurements obtained from individual rotational seismometers show significant deviations with each other and with the array rotation rates in the ranges of 3–5 Hz and, especially, 3–50 Hz. A cross-correlation method was used to compare array-computed rotation rates and point rotation rate measurements in the frequency band of 3–5 Hz with the result that the absolute value of the normalized maximum correlation coefficient for each station set varied from 0.45 to 0.97 with an average of 0.84. Amplitude differences of the point rotation rate measurements are seen to be factors of 0.2 to 1.8 times the array rotations as well. It is not likely that the differences seen in the point and array-computed rotation rates are due to nonlinear or heterogeneous site conditions under each array element since these effects should also be seen in the acceleration data used to determine rotation rate. A rigorous method for accurately calibrating rotation rate instruments is needed to understand their response in the field.

L. M. Kendall (✉) · C. A. Langston
Center for Earthquake Research and Information,
University of Memphis,
3876 Central Avenue, Suite 1,
Memphis, TN 38152, USA
e-mail: lmkndall@memphis.edu

C. A. Langston
e-mail: clangstn@memphis.edu

W. H. K. Lee
862 Richardson Court,
Palo Alto, CA 94303, USA
e-mail: willielee88@gmail.com

C. J. Lin · C. C. Liu
Institute of Earth Sciences, Academia Sinica,
P.O. Box 1-55, Nankang,
Taipei 115, Taiwan
e-mail: youngman@earth.sinica.edu.tw

C. C. Liu
e-mail: ccliu@earth.sinica.edu.tw

Keywords Rotation · Array · TAIGER · Eentec

1 Introduction

Rotational seismology is an emerging field (Lee et al. 2009a, b; Stupazzini et al. 2009). A particular concern is being able to measure rotation rates directly. This has been attempted using instruments such as solid-state devices and ring lasers (e.g., Nigbor 1994; Takeo 1998; Schreiber et al. 2009). Recently, more affordable commercial rotational seismometers have become available that can measure with great sensitivity rotational waves produced from earthquakes, explosions, and other energy sources. In order to effectively use these new instruments, further tests are required by the seismological community to evaluate their accuracy. In this paper, we examine the response of the eentec R-1 rotational seismometer under field conditions that include recording strong ground motions from nearby large explosions. Others have examined the response of eentec R-1 rotational seismometers in the laboratory (Nigbor et al. 2009; Wassermann et al. 2009), but not under field conditions that include siting and installation variables. We will examine seismic waves recorded by the eentec R-1 rotational seismometer and compare them to rotation rates calculated using seismic array "geodesy" (Gomberg et al. 1999) to determine the accuracy of the rotational seismometers. The data come from two large explosions detonated for the Taiwan Integrated Geodynamics Research (TAIGER) (Lin et al. 2009) project in Taiwan on 4 March 2008.

Acceleration data from a dense array of accelerometers are used to calculate wave spatial gradients and resulting rotation and strain rates (Langston and Liang 2008). Langston et al. (2009) used these methods to examine rotation rate as well as strain rate, wave speed, direction, spatial amplitude variation, and stress for the two large TAIGER explosions although they only examined the vertical component of rotation rate (around the local *z*-axis). In this article, we will compute all three components of rotation rate (local *x*, *y*, and *z*) compared to the three component rotational velocity data recorded by the eentec rotational seismometers.

The two TAIGER explosions were detonated about 500 m from the center of the small array (Fig. 1). These explosions, N3P and N3, contained 3,000 and 750 kg of explosives, respectively. Accelerometers and rotational seismometers were positioned close together with 5 m between stations. We will focus on the comparison of each component of rotation rate (or velocity) at each of the five center array stations. There will be 15 waveforms from the rotational seismometers (which will be termed "point rotation rate measurements") and 15 waveforms from array geodesy calculations using data from the accelerometers (which will be termed "array-computed rotation rates") for each of the two explosions for a total of 30 waveforms of each type.

The eentec R-1 rotational seismometer uses a nontraditional left-handed coordinate system for the direction of positive rotation rate. Referring to Fig. 1, our Cartesian coordinate system follows the general right-handed rule, but the direction of positive rotation about the Cartesian axes as recorded by the rotational seismometers follows a left-handed rule. We adopted this convention to make the comparison between point and array-computed rotation rates. We show that the point rotation rate measurements are variable when compared with the computed array rotation rates. The computed array rotation rates are highly correlated with themselves when compared by component, but the point rotation rate measurements are less correlated with the local *x* components having the most variations.

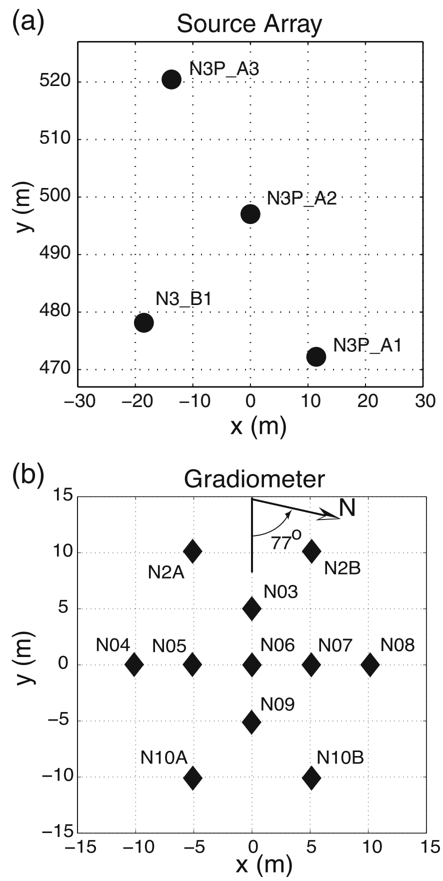

Fig. 1 Source (**a**) and gradiometer (**b**) geometry from Lin et al. (2009). Borehole locations for the N3P and N3 explosions are labeled in **a** where N3P_A3, N3P_A2, and N3P_A1 correspond to the N3P explosion and N3_B1 corresponds to the N3 explosion. Stations are labeled in **b**; we compared rotational waveforms from stations N03, N05, N06, N07, and N09 as they had both a rotational seismometer and an acceleration sensor. Acceleration data from the 11 stations were used to calculate the computed array rotation rates. The direction of positive rotation rate is found using the nontraditional left-handed rule around each of the positive axes (the superimposed Cartesian coordinate system of *x*, *y*, and *z* where *z* is out of the page and station N06 is the center)

Reasons for this result are investigated by comparing results for the two different explosions and through Fourier analysis.

2 Data

The experimental details, setup, and specific calibrations of the TAIGER explosions and of the instrument network are outlined in Lin et al. (2009). Two large explosions were detonated about an hour apart on 4 March 2008; the first one consisted of three simultaneous 1,000 kg borehole explosions (known as N3P) and was detonated at 17:01 UT, and the second explosion contained 750 kg of explosives in one single borehole (known as N3) and was detonated at 18:01 UT. For simplicity, a Cartesian coordinate system is centered at station N06 (Fig. 1) with the middle borehole of the N3P explosion situated about 500 m from the center of the instrument array. Instrument locations N03, N05, N06, N07, and N09 contain both accelerometers and rotational seismometers and are the stations of interest in comparing the two data sets. However, all 11 stations contain accelerometers and each accelerograph of the array is used to compute rotation rates for the five, inner array elements. The array was specifically designed to sample less than 10 % of the target wavelength to accurately compute the wave spatial gradients (Langston et al. 2009). Seven of the stations had Metrozet TSA-100S acceleration sensors and the others had Kinemetrics Episensor ES-T sensors. The five center array elements also had eentec R-1 rotational seismometers with Quanterra Q330 dataloggers. The accelerometers are both force-balanced, and their amplitude responses are flat from 0 to 225 and 200 Hz, respectively (Lin et al. 2009). Factory specifications for the instruments and on-site calibrations are presented in Lin et al. (2009).

3 Theoretical background

Rotation rate is computed using wave spatial gradients obtained from observation of accelerations at each station in the array. The spatial gradients are found by modeling the wavefield through a Taylor's expansion as suggested by Spudich et al. (1995). This process is applied to the acceleration data in order to compute rotation acceleration for each of the three components at each of the five stations and then integrating to obtain rotation rate.

Rotation rate can be related to an incoming wave through its spatial gradient. Rotation rate is calculated relative to a reference point or 'master receiver,' which will be the locations of each accelerometer at stations N03, N05, N06, N07, and N09. The spatial gradient at the master receiver (s_0) can be related to the wavefield at all other receivers (s_i) (Langston and Liang 2008; Liang and Langston 2009):

$$du_i = u_i - u_0 = \delta x_i \frac{\partial u}{\partial x}|_{S_0} + \delta y_i \frac{\partial u}{\partial y}|_{S_0} + du_i^{err} \tag{1}$$

where i=1,2,…,N where N is the number of stations; u can be u_x, u_y, or u_z; and $\delta x_i = x_i - x_0$ and $\delta y_i = y_i - y_0$. We are using the assumption that the error, du_i^{err}, is of second order and can be neglected. In matrix form:

$$Gm = d \tag{2}$$

where

$$G = \begin{bmatrix} \delta x_1 & \delta y_1 \\ \delta x_2 & \delta y_2 \\ \vdots & \vdots \\ \delta x_N & \delta y_N \end{bmatrix}$$

$$m = \begin{bmatrix} \frac{\partial u}{\partial x}\Big|_{s_o} \\ \frac{\partial u}{\partial y}\Big|_{s_o} \end{bmatrix} \tag{3}$$

$$d = \begin{bmatrix} du_1 \\ du_2 \\ \vdots \\ du_N \end{bmatrix}$$

The least-squares solution for the spatial gradients is:

$$m = \left(G^T G\right)^{-1} G^T d \tag{4}$$

The three components of rotation rate about the x-, y-, and z-axes at the Earth's surface are (Lin et al. 2009):

$$\begin{aligned} \omega_x &= \frac{\partial u_z}{\partial y} \\ \omega_y &= \frac{\partial u_z}{\partial x} \\ \omega_z &= -\frac{1}{2}\left(\frac{\partial u_x}{\partial y} - \frac{\partial u_y}{\partial x}\right). \end{aligned} \tag{5}$$

Inserting the proper component of the spatial gradient into Eq. (5) gives the rotation rate about each axis.

4 Data analysis

Units for observed rotation rates are in milliradians per second. The derived array rotation rates start from differencing acceleration using the theory listed in the previous section, in centimeters per square second to obtain radians per square second. The original acceleration records are presented in Langston et al. (2009) in the bands 3–5 and 3–50 Hz. Langston (2007) provides a discussion on the error level associated with calculating spatial derivatives. Rotation acceleration is then time-integrated to obtain rotation rate using the Fourier integral theorem and then scaled to obtain milliradians per second. We then convolved the nominal eentec R-1 rotational sensor instrument response into the computed array rotations to compare them with the point rotation rate data. We also applied a 3–5 Hz frequency bandpass filter after multiplying them by negative one to account for the nontraditional direction of positive rotation.

Ideally, the point rotation rate measurements should be identical to the computed array rotation rates as they both are recordings of the rotational waves from the two large explosions. The rotation rates at each of the five stations should have the same shape because the horizontal seismic wavelength in our assumed bandpass is greater than the array aperture of 10 m. For example, a 4-Hz P wave with a horizontal phase velocity of 4,000 m/s would have a horizontal wavelength of 1,000 m which is much greater than the array diameter (Langston et al. 2009). This is the reason for choosing the 3–5 Hz bandpass. This relatively low frequency bandpass is well within the responses of both the accelerometers and the eentec R-1 rotational seismometer while preserving the requirement that the array aperture be 10 % or less than the observed seismic wavelengths.

Point and array rotation rates were plotted by explosion (N3P and N3) and then by the local *x*-, *y*-, and *z*-axes (Fig. 2). The point rotation rate measurements have noticeable amplitude and phase differences. The superimposed computed array rotation rates, on the other hand, show very little variation. This indicates two things: First, the array-computed rotation rates are quite stable because they show almost no variation over the array. This consistency of rotation rate estimates, even using different reference points for the Taylor series inversion, is consistent with the expected wave propagation. Long-wavelength seismic waves should not change amplitude or phase over relatively short distance ranges. Secondly, but much more problematical, the rotational sensor waveforms have small time shifts and amplitude variations among themselves and when compared to the "correct" array-derived rotation rates. Largest waveform variations occur for the *x* components of stations N06 and N09.

In an attempt to quantify the differences in the point rotation rate measurements, cross-correlation of the point and array rotation rates was applied to the filtered waveforms for each component of each station. We were interested in waveform similarity, given by the maximum of the normalized cross-correlation, the time shift that gave the maximum normalized cross-correlation, and the amplitude of the un-normalized cross-correlation at zero time shift (Table 1). The absolute values of the normalized cross-correlation coefficients range from 0.45 to 0.97 with an average of 0.84. The optimum, least-squares estimate of the amplitude variation of the un-normalized cross-correlations is represented by:

$$A = \frac{[O(t) \otimes S(t)]_{\tau=0}}{[S(t) \otimes S(t)]_{\tau=0}} \tag{6}$$

where the circled cross denotes the cross-correlation, $O(t)$ is the point rotation rate measurement, and $S(t)$ is the computed array rotation rate (Langston et al. 2002).

Our first comparison was to simply divide each point rotation rate measurement by its inferred amplitude variation value. The new, "corrected" waveforms were then superimposed on the computed array rotation rates (Fig. 3). With these corrections, the waveforms become more similar for the *y* and *z* components, but the *x* component waveforms still vary wildly.

We then investigated spectral amplitude ratios of the observed point rotation rates compared to the array rotation rates to see if there were consistent characteristics that could be attributed to differences in spectral instrument response among the rotational seismometer channels. First, all of the waveforms were transformed into the frequency domain using an FFT. The number of points in the time series is 6001, so the corresponding frequency resolution is 0.03 Hz. The amplitude spectra

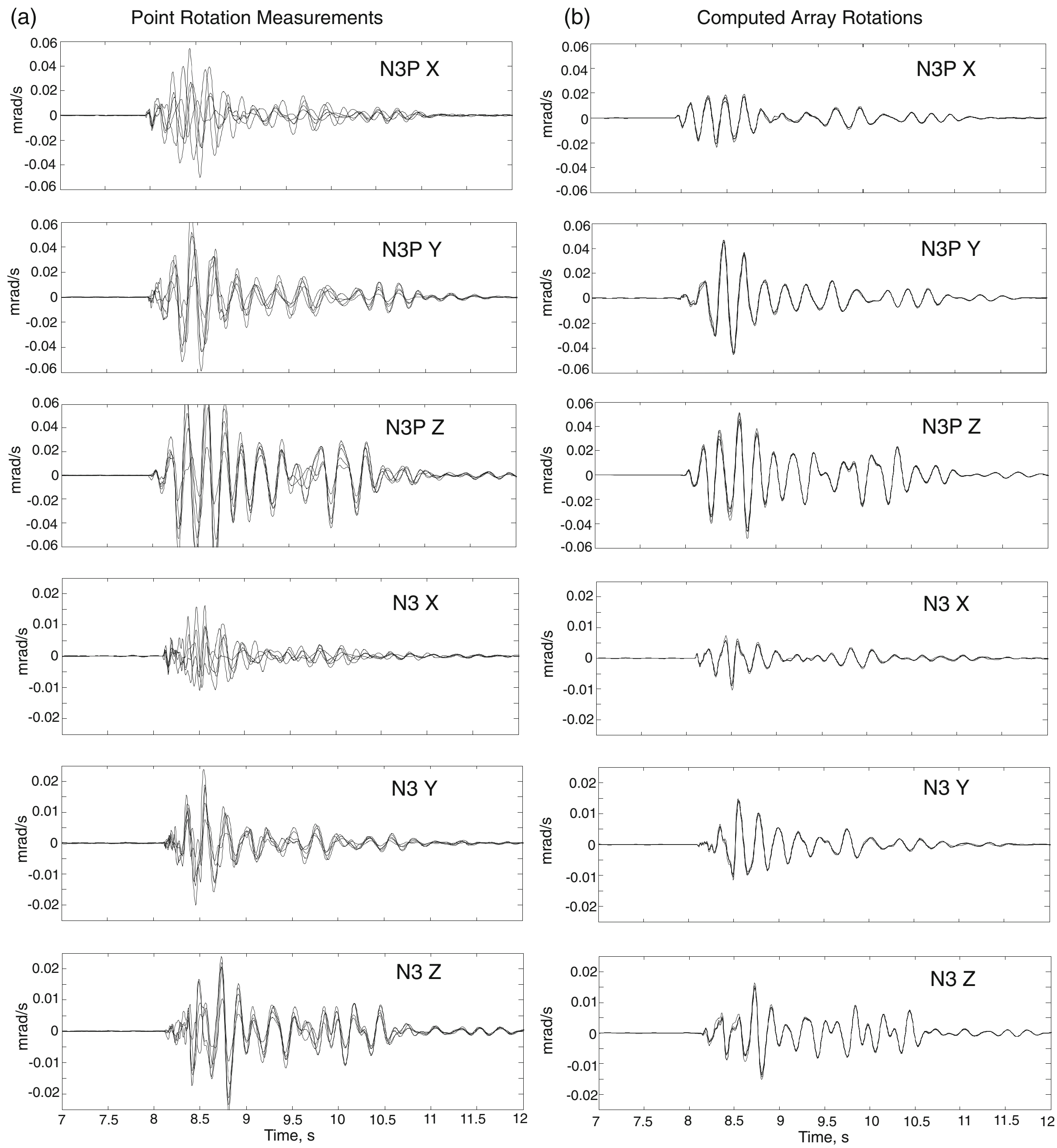

Fig. 2 Local x, y, and z components of rotation rate for each of the explosions with the measurements at the five stations superimposed in the frequency range 3–5 Hz. Point rotation rate measurements (**a**) show considerable variations and are distinguishable from each other while the computed array rotation rates (**b**) show such little variation that the five waveforms plotted are almost indistinguishable

were smoothed using a running average of 10 points (or 0.3 Hz) on either side of the center frequency (Fig. 4) in order to avoid irregularities and zeros which would cause spectral ratios to have spurious peaks. After smoothing, spectral ratios of the point to array rotation rates for each component of each station were computed (Fig. 5).

Most z channels show a resonance peak at about 4.1 Hz that can increase observed rotation rate amplitudes

Table 1 Quantifying waveform similarity

Explosion N3P				Explosion N3			
Station+ component	Normalized maximum cross-correlation coefficient	Lag at maximum cross-correlation coefficient (s)	Amplitude ratio at zero lag	Station+ component	Normalized maximum cross-correlation coefficient	Lag at maximum cross-correlation coefficient (s)	Amplitude ratio at zero lag
3 *X*	0.92	−0.02	0.86	3 *X*	0.84	0.00	0.91
3 *Y*	0.97	0.02	0.73	3 *Y*	0.94	0.00	0.94
3 *Z*	0.94	0.01	1.41	3 *Z*	0.85	0.01	1.24
5 *X*	0.88	−0.04	0.89	5 *X*	−0.74	−0.13	0.81
5 *Y*	−0.89	−0.12	1.22	5 *Y*	−0.86	−0.12	1.15
5 *Z*	0.85	0.01	0.53	5 *Z*	0.84	0.01	0.60
6 *X*	−0.60	0.21	−0.99	6 *X*	0.45	−0.10	−0.47
6 *Y*	0.76	0.01	0.35	6 *Y*	0.83	0.01	0.45
6 *Z*	0.95	0.01	1.81	6 *Z*	0.88	0.01	1.37
7 *X*	0.82	−0.02	0.70	7 *X*	−0.76	0.07	0.62
7 *Y*	−0.92	−0.12	1.01	7 *Y*	0.85	0.00	0.89
7 *Z*	0.95	0.02	1.03	7 *Z*	0.89	0.01	0.97
9 *X*	−0.77	−0.07	0.26	9 *X*	0.70	0.03	0.22
9 *Y*	−0.93	−0.11	1.06	9 *Y*	−0.88	−0.11	1.00
9 *Z*	0.93	0.00	1.46	9 *Z*	0.87	0.01	1.22

This table presents a quantifiable comparison of the rotation rate waveforms of each component and explosion using normalized maximum cross-correlations and amplitude variations. The lag at the maximum normalized cross-correlation gives the time shift of the waveforms

by factors of 2 to 4 (Fig. 5). *Y* channels seem best behaved with more subdued resonance peaks and spectra that suggest a response within 50 % of advertised values. *X* channels show the greatest variation in spectral ratios with the appearance of large resonance peaks near 4.3 Hz that amplify rotational motions by up to factors of 10. Notably, station 3 *x* component spectral ratios are comparable to the better *y* components. Spectral ratios for each event are similar, but the smaller explosion, N3, seems to have greater resonance peaks than the larger explosion, N3P.

5 Discussion

A field experiment of this type potentially contains many more variables that may affect seismic recordings than would normally occur in more controlled laboratory conditions. It is natural to suspect that very local site and wave coupling conditions under each instrument could affect both the acceleration and rotation rate measurements. The experiment was performed in the Lan-Yang river valley with hills, roads, and a cultivated field nearby (Lin et al. 2009). Photographs of individual array elements show that concrete pads were poured over a heterogeneous mix of river gravels and large cobbles. Perhaps this kind of site heterogeneity gave rise to very local wave scattering, base resonance, or some other unknown, nonlinear condition to cause substantial variations between rotational seismometer recordings.

The eentec rotational sensors themselves were tested before the experiment, and the sensitivity values obtained were off by as much as 30 % from the factory specifications (Lin et al. 2009). However, the method used was approximate; Lin et al. (2009) states that "… this method determines the average sensitivity over several frequency bands, so that the total frequency response cannot be obtained." Nominally, the response of the eentec R-1 is flat to rotation rate between 0.05 and 20 Hz. The data comparisons of Figs. 2, 3, and 5 show that there is considerable variation among the rotation channels of the array. What is the most likely source of these variations?

The array accelerations offer a strong clue. The wavefield in the 3–5-Hz frequency band is very consistent over all elements of the strong-motion array (Langston

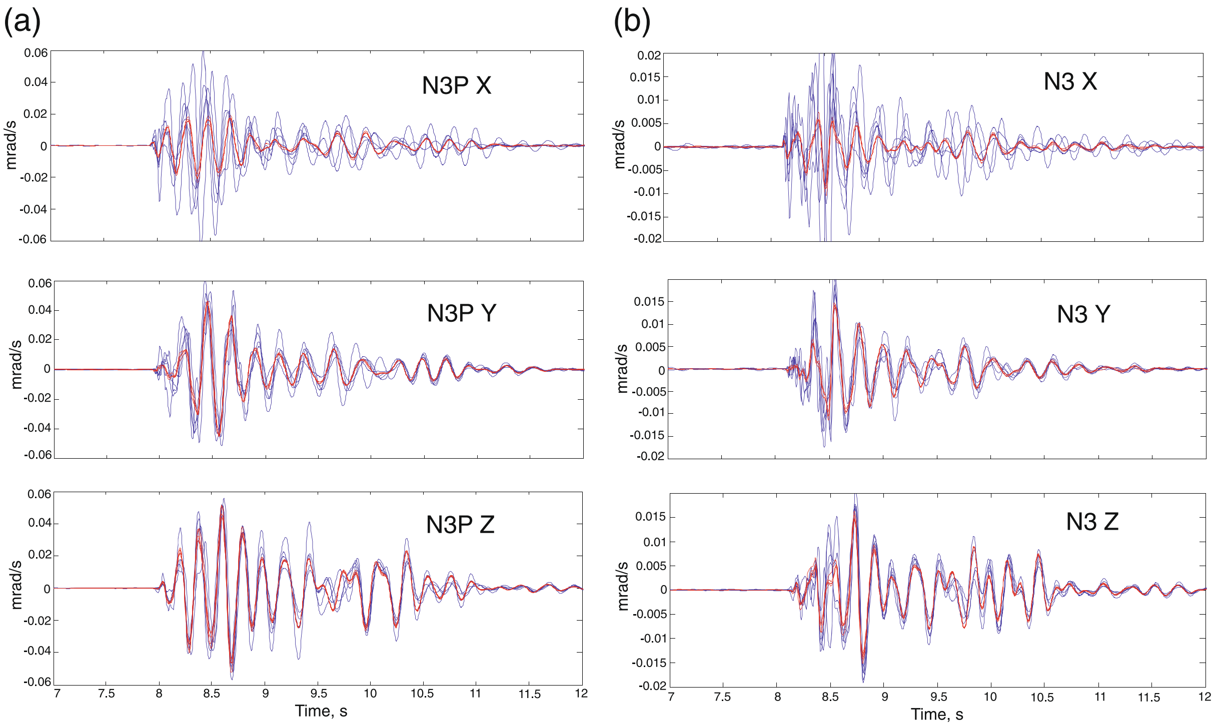

Fig. 3 Superimposed corrected point rotation rate measurements (corrected by dividing the original point rotation rate measurements by the amplitude ratio value from Table 1) and computed array rotation rates for explosion N3P (**a**) and explosion N3 (**b**). The blue waveforms are the corrected point rotation rate measurements, and the red waveforms are the computed array rotation rates. Notice the similarities of the y and z components and the wild amplitude variations of the x component waveforms, specifically at stations N06 and N09

et al. 2009). Furthermore, the computed array rotation rates using the geodetic technique are equally consistent over each rotation element of the array (Fig. 2). If there were some local site resonance or nonlinear effect at each station of the array, these effects should be seen in causing variation among the computed array rotation rates. Instead, both the accelerations and array rotation rates show what would be expected if ground motions are sampled over distance scales much less than a seismic wavelength. Even in the presence of site heterogeneity, the horizontal seismic wavelengths are simply too large to detect small-scale heterogeneity of a few meters or less. The acceleration and array rotation rate data are consistent with long-wavelength wave propagation.

For completeness, we also applied a 3–50 Hz frequency bandpass filter to the rotation rate data to show the high frequency component of the waveforms (Fig. 6). This gave the results that we expected: The waveforms are less correlated in the higher band than in the 3–5 Hz range. This is because the waves included in the 3–50 Hz band are shorter period, so the original requirement that the array aperture sample less than 10 % of a wavelength is not honored. The point rotation rate measurements show large amounts of variability within the small time window of 0.4 s in Fig. 6. This is the reason the 3–5 Hz bandpass frequency was used in the analysis of this paper: The waves being sampled are greater than ten times the array aperture, so the array-computed waveform calculations are accurate, and they can be correctly compared to the point rotation rate waveforms.

We considered the effect that rotation could have on the acceleration recordings themselves to estimate any bias that might occur in using acceleration data contaminated with tilts and rotations. It is well-known that horizontal seismographs are sensitive tilt meters. Horizontal component strong-motion accelerometers will be directly affected by a component of gravity through g where g is the gravitational acceleration and $\ll 1$ is the tilt or rotation about a perpendicular horizontal axis. However, the horizontal rotations are functions of the vertical acceleration through Eq. (5). Vertical

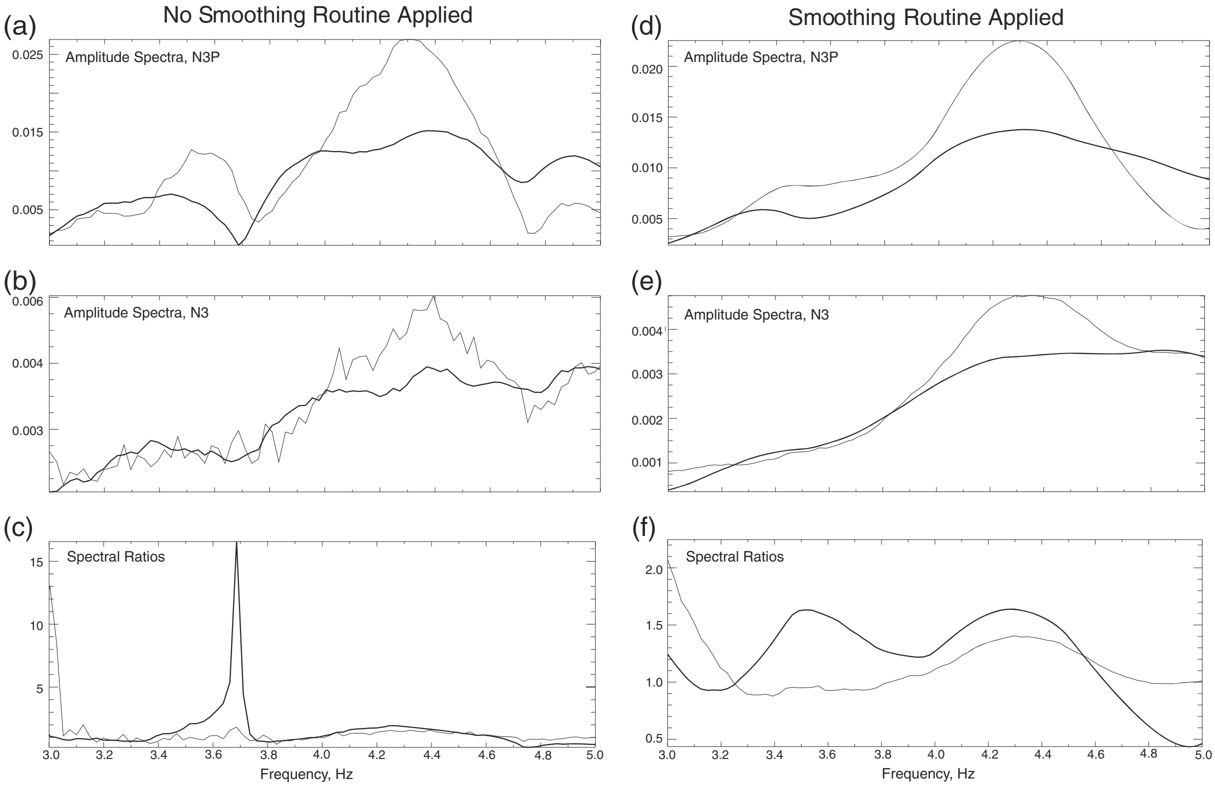

Fig. 4 Component *y* from station N06 is shown to illustrate the benefit of using a smoothing operator. For this figure and Fig. 5, a running average of ten points on either side of the center frequency was applied (Goldstein et al. 2003). Amplitude spectra (**a**, **b**, **d**, **e**) are shown with (*right-handed column*) and without (*left-handed column*) smoothing applied where the *thick lines* are the array-computed rotation rates and the *thin lines* are the point rotation rate measurements. Notice how a smoothing routine filters out the discontinuities. The spectral ratios (**c**, **f**) are shown with and without smoothing where the *thick line* represents explosion N3P and the *thin line* represents explosion N3. The spectral ratios were calculated with the point rotation rate measurements divided by the array-computed rotation rates

acceleration is insensitive to tilt, to first order but would be more sensitive to contamination with a small component of horizontal acceleration being detected by the tilted vertical accelerometer. However, the largest rotation rates are of the order of 1 mrad/s which would only cause a contamination of approximately 0.1 % in cross axis ground motion. Furthermore, Grazier (2005) showed that within a limited frequency band, the long-period errors introduced by tilting are eliminated.

Both the variation in waveform and variation in spectral characteristics among the channels of the rotational seismometer array strongly suggest that the variation is due to variations in the instrument responses (Figs. 2, 3, and 5). The *x* and *z* component data show similar spectral resonances near 4.0–4.3 Hz for both explosion sources. It is also interesting to observe that spectral ratio data for the smaller event that occurred 1 h after the large explosion show higher amplitude ratios with the array-computed rotation rates. Perhaps the sensors sustained mild damage during the large explosion. Investigating these conjectures is beyond the purpose of this report.

Another reason for the waveform variation that needs to be explored in future studies is amplitude distortion. The output response we are analyzing in this paper could be a nonlinear function of the input wave amplitude. If these were the case, just removing the linear instrument response would not fix the variations seen in the point rotation rate measurements. Investigating nonlinearity requires controlled input signals where amplitude and signal phase can be varied to explore the resulting output. It has been suggested that there might be distortion effects in the rotational seismometers that starts at 20–40 % of full scale (Nigbor, personal communication, November 12, 2011). The clip level of the rotational

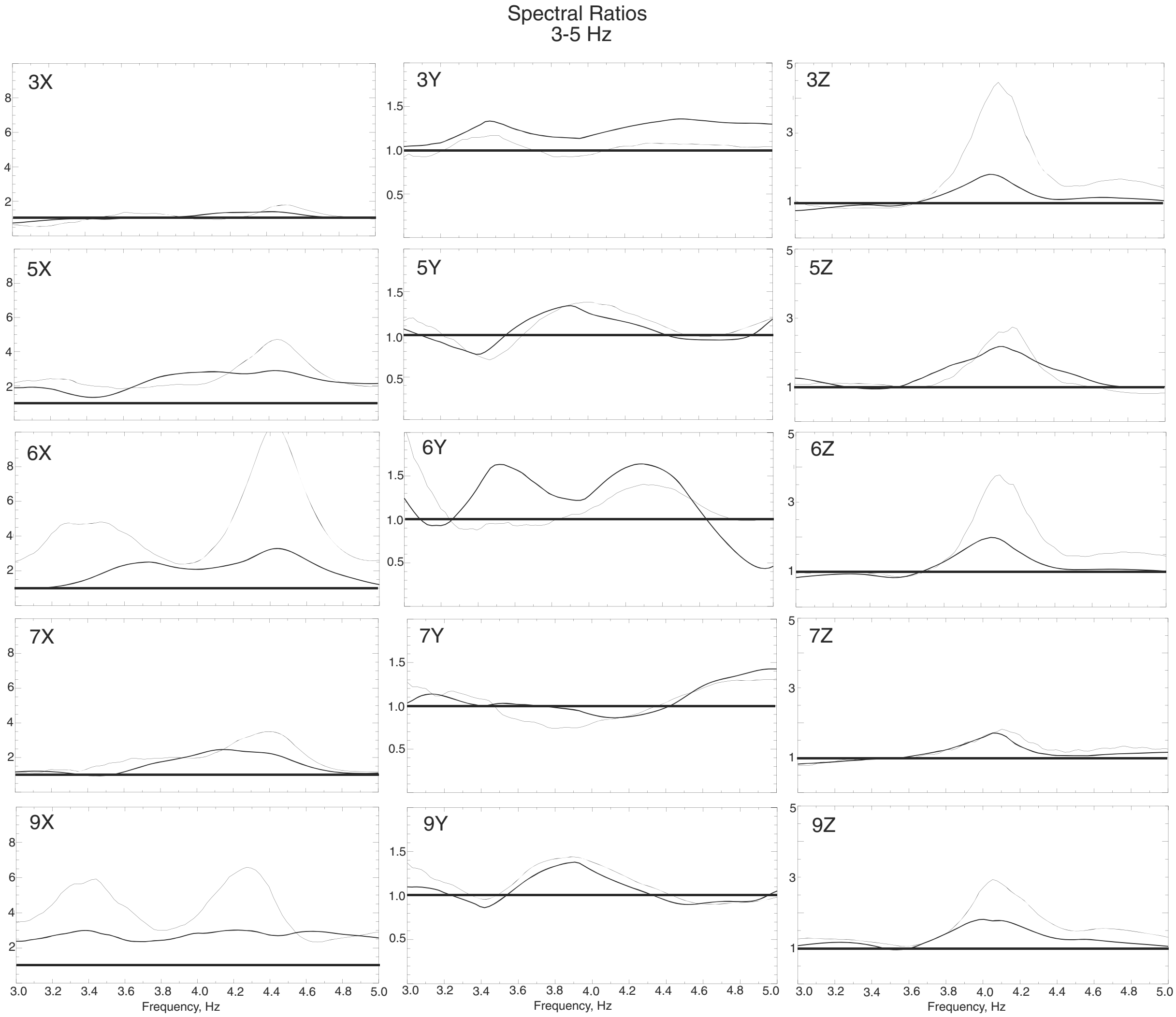

Fig. 5 Unit-less spectral ratios of the point rotation rate measurements to the array-computed rotation rates for each explosion at each of the five stations in the range of 3–5 Hz. Each plot contains the spectral ratio from both explosions and is separated by station component. The *thicker line* is for the N3P explosion and the *thinner line* for the N3 explosion. The *horizontal line* denotes a ratio of one. Note that the amplitude scale is the same for each component but changes between components

seismometers is 1 rad/s at 1 Hz (eentec specification sheet). The waveforms shown in this paper have amplitudes of up to 1.5 mrad/s which is only 1.5 % of full scale, far from 20 % to 40 % of the maximum output of the instrument.

After correction by the inferred amplitude ratio found from the zero-lag cross-correlation (Table 1), the point data waveforms generally agree with the array rotation rates, except for the *x* components at stations N06 and N09 (Fig. 3). This suggests that a rigorous testing program is required before fielding these instruments to determine more accurate instrument responses. One such method might involve a long-duration "huddle" test where instruments are grouped closely to each other on a solid pad. Recordings of high amplitude ambient noise could be used to determine accurate relative rotation rate responses using techniques suggested by Pavlis and Vernon (1994).

6 Conclusions

Acceleration-derived geodetic rotation rates and point rotation rate data recorded by eentec R-1 rotational seismometers after two large explosions in northeastern Taiwan were successfully compared. Computed array rotation rate showed little variation over the five array stations, consistent with long-wavelength seismic wave propagation. However, the point rotation rate measurements showed considerably more variation among themselves and when compared to the array rotation rates quantified by normalized cross-

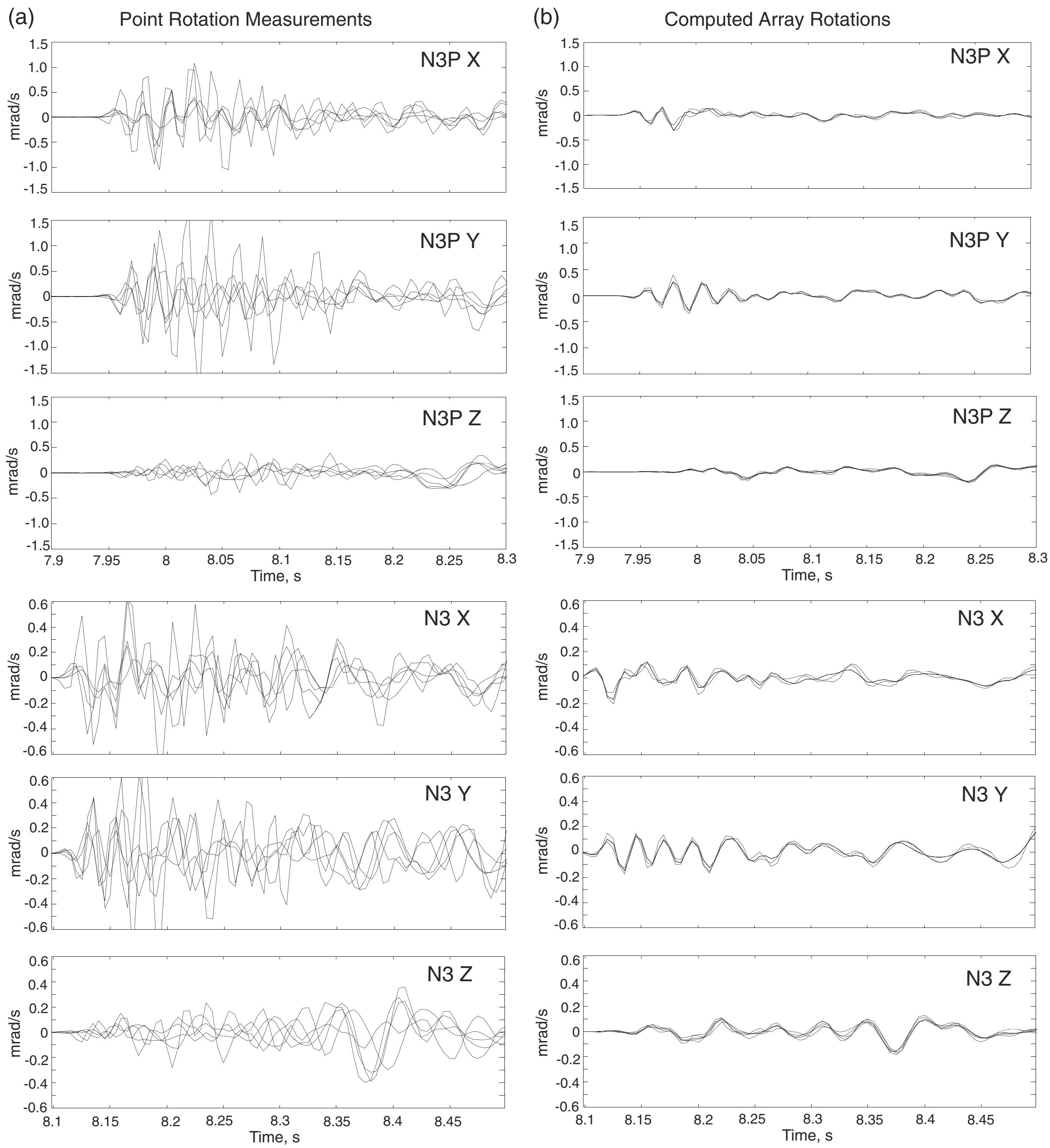

Fig. 6 Local *x*, *y*, and *z* components of rotation rate in the 3–50-Hz range with the five waveforms at each station superimposed. The waves shown are the first 0.4 s of motion, and there is a change in the times from the N3P to N3 explosions. The point rotation rate measurements (**a**) show large variations with one another—even more than in Fig. 2. The array-computed rotation rates (**b**) show more variations with each other compared to the low frequency bandpass because these short period waves have wavelengths that are less than ten times the array aperture, which increases the error in computed array rotation rates

correlation coefficients, amplitude variation at zero cross-correlation lag (Table 1), and ratios of the spectra of point to array rotation rates.

The absolute value of the normalized cross-correlation values between the two sets of rotational waveforms in the frequency band 3–5 Hz had an average of 0.84. Spectral analysis showed that the spectral ratios varied by component and often had large resonance peaks near 4.0–4.3 Hz. The *x* components of two stations (N06 and N09) were particularly problematical. Variations in the observed point rotation rate data are attributed to variations in instrument response and not site heterogeneity.

Acknowledgments We would like to thank the Center for Earthquake Research and Information at the University of Memphis for funding support. The manuscript was improved by comments made by two anonymous reviewers.

Data and resources All translational and rotational seismograms described in this paper were collected by Chin-Jen Lin, Chun-Chi Liu, and William H. K. Lee and are archived on the website of the International Working Group on Rotational Seismology (http://www.rotational-seismology.org, last accessed July 2011). Seismic Analysis Code (Goldstein et al. 2003) and MATLAB (matrix laboratory) were used in the data processing and are gratefully acknowledged.

References

Goldstein P, Dodge D, Firpo M, Minner L (2003) SAC2000: signal processing and analysis tools for seismologists and engineers. In: Lee WHK, Kanamori H, Jennings PC, Kisslinger C (eds) The IASPEI international handbook of earthquake and engineering seismology. Academic, London

Gomberg J, Pavlis G, Bodin P (1999) The strain in the array is mainly in the plane (waves below 1 Hz). Bull Seismol Soc Am 89(6):1428–1438

Grazier VM (2005) Effect of tilt on strong motion data processing. Soil Dyn and Earthq Eng 25:197–204

Langston CA (2007) Spatial gradient analysis for linear seismic arrays. Bull Seismol Soc Am 97(1B):265–280

Langston CA, Liang C (2008) Gradiometry for polarized seismic-waves. J Geophys Res 113:B08305

Langston CA, Nyblade AA, Owens TJ (2002) Regional wave propagation in Tanzania, East Africa. J Geophys Res 107: B1. doi:10.1029/2001JB000167

Langston CA, Lee WHK, Lin CJ, Liu CC (2009) Seismic-wave strain, rotation, and gradiometry for the 4 March 2008 TAIGER explosions. Bull Seismol Soc Am 99(2B):1287–1301

Lee WHK, Huang BS, Langston CA, Lin CJ, Liu CC, Shin TC, Teng TL, Wu CF (2009a) Review: progress in rotational ground-motion observations from explosions and local earthquakes in Taiwan. Bull Seismol Soc Am 99(2B):958–967

Lee WHK, Igel H, Trifunac MD (2009b) Recent advances in rotational seismology. Seismol Res Lett 80(3):479–490

Liang C, Langston CA (2009) Wave gradiometry for USArray: Rayleigh waves. J Geophys Res 114. doi:10.1029/2008JB005918

Lin CJ, Liu CC, Lee WHK (2009) Recording rotational and translational ground motions of two TAIGER explosions in northeastern Taiwan on 4 March 2008. Bull Seismol Soc Am 99(2B):1237–1250

Nigbor RL (1994) Six-degree-of-freedom ground-motion measurement. Bull Seismol Soc Am 84(5):1665–1669

Nigbor RL, Evans JR, Hutt CR (2009) Laboratory and field testing of commercial rotational seismometers. Bull Seism Soc Am 99:1215–1227

Pavlis GL, Vernon FL (1994) Calibration of seismometers using ground noise. Bull Seism Soc Am 84:1243–1255

Schreiber KU, Hautmann JN, Velikoseltsev A, Wassermann J, Igel H, Otero J, Vernon F, Wells JPR (2009) Ring laser measurements of ground rotations for seismology. Bull Seism Soc Am 99:1190–1198

Spudich P, Steck LK, Hellweg M, Fletcher JB, Baker LM (1995) Transient stresses at Parkfield, California, produced by the M 7.4 Landers earthquake of June 28, 1992: observations from the UPSAR dense seismograph array. J Geophys Res 100:675–690

Stupazzini M, Puente J, Smerzini C, Kaser M, Igel H, Castellani A (2009) Study of rotational ground motion in the near-field region. Bull Seismol Soc Am 99(2B):1271–1286

Takeo M (1998) Ground rotational motions recorded in near-source region of earthquakes. Geophys Res Lett 25 (6):789–792

Wassermann J, Lehndorfer S, Igel H, Schreiber U (2009) Short note: performance test of a commercial rotational motions sensor. Bull Seismol Soc Am 99(2B):1449–1456